J Mater Sci (2010) 45:2892–2901
DOI 10.1007/s10853-010-4280-3

Morphology, mechanical and thermal properties of nano-structured full IPNs based on polyisoprene and PMMA

Jacob John · R. Suriyakala · Selvin Thomas · Jude Martin Mendez · Anitha Pius · Sabu Thomas

Received: 8 December 2009 / Accepted: 25 January 2010 / Published online: 18 February 2010

Abstract Morphology, mechanical properties, thermal stability and gas transport behaviour of interpenetrating polymer networks (IPNs) based on PI/PMMA have been investigated using various techniques. Crosslinking level of both phases and concentration of PMMA were found to have noticeable effects on the compatibility of immiscible components during IPN formation. Effect of crosslinking was studied by preparing IPNs with varying amount of crosslinker concentration in each phase. Crosslinking of both phases facilitated deeper interpenetrations between both networks, and certain degree of compatibility is attained during IPN formation. Nanometre-sized domains were observed for highly crosslinked IPN. Lower concentration of PMMA was found to favour phase mixing more effectively than others. DSC curve of 65/35 IPN showed a broad transition arising from the α and β-relaxations of PMMA due to the higher flexibility attained by mixing with the highly mobile PI chains. The mechanical properties of the IPNs were correlated to the morphology of the system and 50/50 composition showed maximum mechanical properties among the studied compositions. Mode of mechanical failure, thermal stability and gas transport behaviour were also analysed. IPNs having nanometre-sized domains showed least gas permeability among the studied samples.

J. John · A. Pius (✉)
Department of Chemistry, Gandhigram Rural University, Dindigul, Tamil Nadu 624302, India
e-mail: dranithapius@gmail.com

J. John
e-mail: jacobparayil@gmail.com

R. Suriyakala
Polymer Science and Engineering, University of Massachusetts, Amherst, MA 01002, USA

S. Thomas
Corporate R & D Division, HLL Lifecare Limited, Karamana, Trivandrum 695002, India

J. M. Mendez
Department of Chemistry, St. Albert's College, Ernakulam, Kerala, India

S. Thomas (✉)
School of Chemical Sciences, Mahatma Gandhi University, Kottayam, Kerala 686560, India
e-mail: sabuchathukulam@yahoo.co.uk

Introduction

The preparation, properties and characterization of multicomponent polymeric materials have received considerable interest in recent years. Among these materials, much attention has been given to interpenetrating polymer networks (IPNs). IPNs are defined as a combination of two or more polymers in network form, at least one of which was polymerized and/or cross-linked in the immediate presence of the other. IPNs can be prepared by simultaneous polymerization, sequential polymerization or latex blending technique [1, 2]. The idea is to effect a molecular interpenetration of the networks; in practice, most IPNs form immiscible compositions, usually phase separating during some stage of the synthesis. However, due to their interlocking phase configuration, the extent of phase separation is restricted, and domain dimensions are on the order of hundred or tens of nanometres [3, 4]. IPN synthesis is highly significant and interesting because it is the only way

of mixing two cross-linked polymers intimately. While the different morphologies in block polymers are well investigated, the exact prediction of the phase shape and phase continuity is difficult in the case of IPNs [5].

For sequential IPNs, two theories based on thermodynamic consideration exist, both predict spherical domains of polymer II and hence a discontinuous polymer II phase [6]. However, the evidence against dual phase continuity was not satisfactorily established since DMTA results suggested dual phase continuity [7]. Morphology developed during full IPN synthesis ultimately determines the mechanical performance of these materials.

If two polymers A and B are incompatible and the crosslinking density of A is low, i.e., the molecular weight between cross-links is high, then during the polymerization of polymer B, the growing B chains will push apart the already existing A chains, and a phase-separated IPN will be obtained. However, if the cross-linking density of A is high, the positions of the A chains will hardly be changed, and the B polymer will grow interpenetrating the existing network A. Thus, a compatible IPN can eventually be obtained, achieving a forced compatibilization of both polymers to some extent [8–10]. Thus, crosslinking density of the system strongly influences the phase morphology of IPNs due to competitive process between the natural tendency of phase separation and its impossibility due to network formation and consequent appearance of chemical crosslinks. As a result, the physical and mechanical properties of a given IPN can be modified by varying (among other factors) the crosslinking density, and this is precisely the main reason for the growing interest in this kind of materials [11–18].

In this article, we present an extensive analysis on the morphology of IPNs with special emphasis on the effect of composition and crosslink densities of polyisoprene and PMMA by SEM, TEM and SAXS measurements. The mechanical properties, thermal stability and gas transport properties of the IPNs are also analysed.

Experimental

Materials

High molecular weight polyisoprene (PI) ($M_w \sim 500{,}000$) is supplied by Rubber Research Institute India, (RRII). Cross-linkers for PI, Dicumyl Peroxide (DCP 99%) is purchased from Aldrich and used as such. Methyl methacrylate (MMA, Aldrich) and crosslinker ethylene glycol dimethacrylate (EGDMA) were distilled under vacuum prior to use. Azobisisobutyronitrile (AIBN) (Aldrich) was purified by recrystallization from methanol.

Preparation of IPNs

Cross-linked polyisoprene (DCP) sheets (1–2 mm thick) were weighed and kept immersed in a homogeneous mixture of methyl methacrylate, EGDMA and AIBN (0.7 g per 100 g of MMA). The PI sheets were swollen at different time intervals to obtain different weight percentages of PMMA. The swollen samples were kept at 0 °C for a few hours to achieve equilibrium distribution of the MMA monomer in the matrix. These swollen networks were heated at 80 °C for 6 h and at 100 °C for 2 h in an atmosphere of MMA to complete the polymerization and crosslinking of MMA (PMMA $M_w = 733{,}000$, and PDI = 3.09 from GPC). The obtained IPNs were kept in a vacuum air oven to make it free of unreacted MMA. The final weight of the IPN was taken and composition of the sample was determined. (Sample nomenclature: $^{a}NIM^{b}_{c}$, a—crosslinker concentration in PI (wt%), b—crosslinker concentration in PMMA, c—PMMA content in wt%).

Characterization

Scanning electron microscopy (SEM) analyses were performed with a JEOL JSM 6320F Field Emission Gun Scanning Electron Microscope. The samples were cryo-fractured and surface of IPN is coated with Platinum using a Gatan HR 681 Ion beam coater. SAXS profiles were obtained with the beam of incident on the sample surface at 90°. The scattering arising from the sample was recorded on an area detector. X-ray scattering was performed with Ni-filtered Cu-K α radiation from a Rigaku rotating anode, operated at 8 kW. The mechanical properties of the IPNs were measured with Shimadzu AG II universal testing machine. The tensile properties were measured with dumbbell-shaped specimens according to ASTM D-80. Thermal stabilities of the samples were analysed in TGA 2950, TA Instruments Inc. at a heating rate of 10 °C/min from 30 to 600 °C in nitrogen atmosphere. T_gs of IPNs were determined using DSC Q100, TA Instruments Inc. in nitrogen atmosphere at a heating rate of 20 °C/min. The gas permeability of the IPNs was measured using Lyssy Manometric Gas Permeability Tester L100-2402. The test gas used was oxygen at a rate of 10 mL/min. Permeability of the samples was calculated using the equation:

$$P_m = (T_r P_r)/t_m, \quad (1)$$

where P_m is the permeability of the test sample, t_m the interval time constant for the test sample, P_r the permeability of the reference (standard PET sample), T_r the interval time constant for standard PET.

Results and discussion

Morphology

Effect of composition

The solid-state organisation of multicomponent polymeric materials is very important since most of the useful properties of the materials are determined by the morphology of the system. In this report, we present the analysis of a series of full IPNs with different compositions, cross-link densities and attempt has been made to correlate the mechanical performance of the material with the morphology obtained during IPN synthesis. Figure 1a–d shows the SEM images of full IPNs with same cross-link density for both components and having different PMMA concentrations ranging from 20 to 60 wt%. All the four samples showed phase separation with different morphologies clearly depicting the quantitative influence of second component on the morphology developed during IPN synthesis. In sample with 20 wt% of PMMA, Fig. 1a, the PMMA phase was highly dispersed in the continuous polyisoprene matrix showing the characteristic sea-island morphology. In Fig. 1b, also the PMMA phase was in a dispersed state with larger domain dimension than previous one. When PMMA concentration was 50 wt%, the system showed a shift from sea-island morphology to dual phase morphology, however, the polyisoprene phase seems to be the more continuous phase and forms the matrix. At 60 wt%, both phases becomes co-continuous as shown in Fig. 1d.

In IPNs, the phase synthesised first forms the more continuous phase and tends to control the morphology. IPN with 20 wt% PMMA showed a fine structure with PMMA domains dispersed all over PI matrix. As the concentration of PMMA increased, the size of PMMA domains also increased and was found to form clusters of large domains surrounded by very small domains. The sea-island morphology was exhibited by samples with less than 30 wt% of PMMA. The DMA analysis revealed that both the above composition showed higher miscibility when compared to other PMMA compositions. Also, IPN of the above composition showed higher degree of phase mixing than the semi IPNs of the same compositions due to deeper interpenetration of phases resulting from the crosslinking effect of the second phase [19]. According to a theory developed by Sperling [2], in the case of sequential IPN, polymer II that is formed in a swollen network I, constitute a spherical core and is in a contracted (deformed) state, while polymer I surrounds the core and is in an expanded state. This clearly depends on the concentration of the second component and

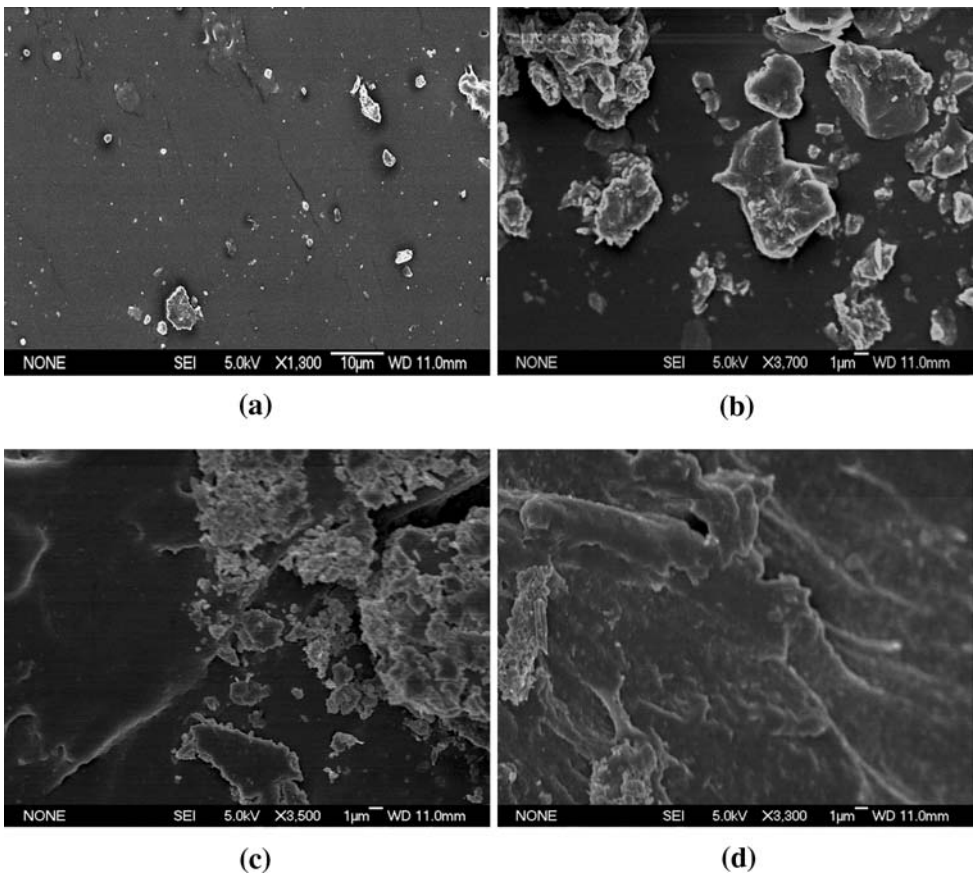

Fig. 1 SEM images of IPNs with same crosslink density and varying compositions. **a** $^{0.8}NIM^{4}_{20}$, **b** $^{0.8}NIM^{4}_{35}$, **c** $^{0.8}NIM^{4}_{50}$, **d** $^{0.8}NIM^{4}_{60}$

when it increases and reaches certain limit, polymer II also becomes continuous as polymer I. This can be noticed in the SEM image of IPN with 60 wt% of PMMA (Fig. 1d).

Effect of cross-link densities of both components

Figure 2a–h shows the SEM images of full IPNs with varying crosslink densities for both components. Figure 2a, b shows full IPNs with higher crosslinks in PI (2%) and lower in PMMA (2%) compared to the above said IPNs shown in Fig. 1a–d. As we mentioned earlier, in the case of sequential IPNs, the first formed phase have an upper hand in controlling the morphology. This was clearly understood from the SEM images. The higher crosslinking of PI matrix resulted in the formation of much smaller, ordered and compact PMMA phase. As the crosslinking level increased,

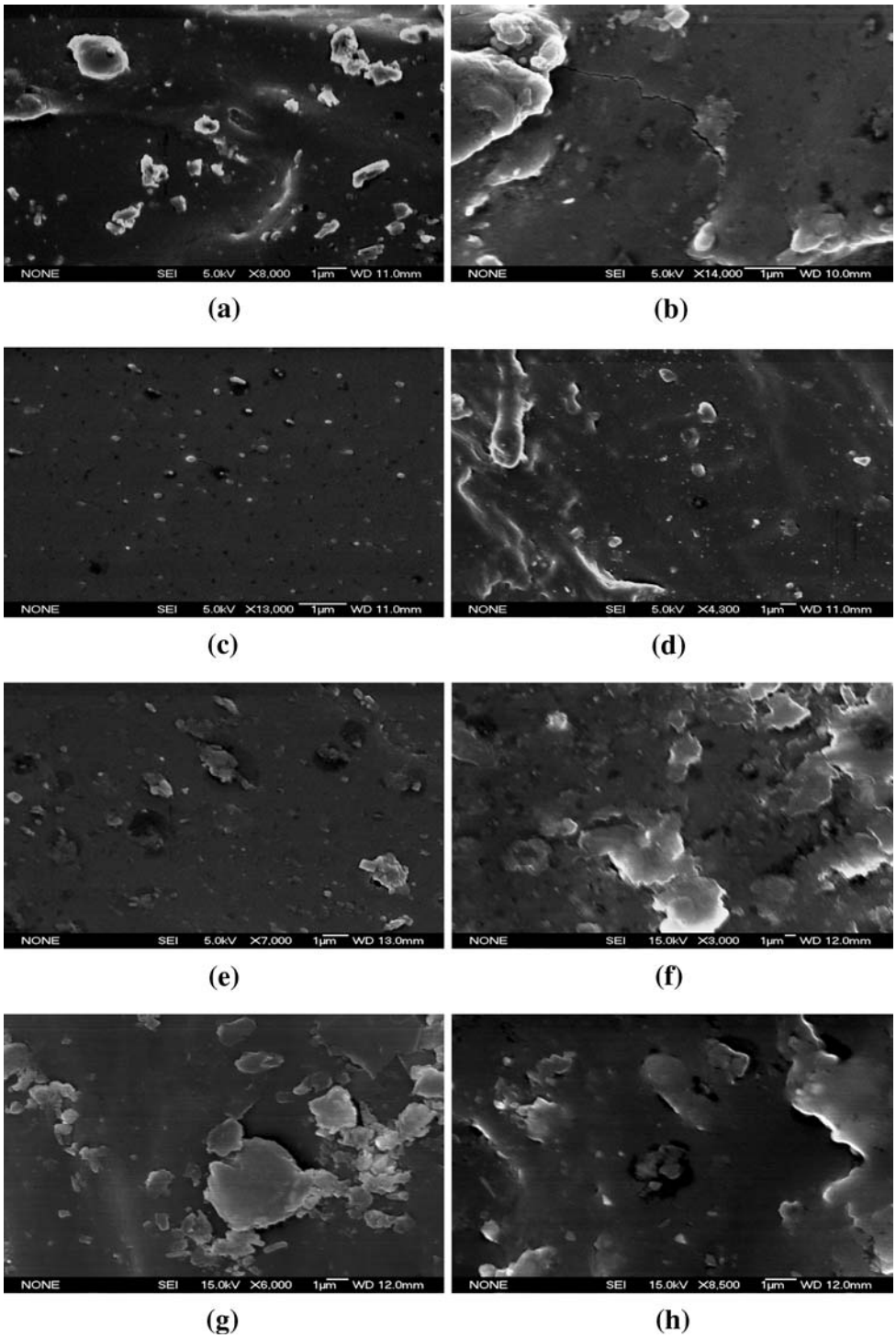

Fig. 2 SEM images of IPNs with different crosslink densities of PI and PMMA. **a** $^{2}NIM^{2}_{35}$, **b** $^{2}NIM^{2}_{50}$, **c** $^{2}NIM^{4}_{50}$, **d** $^{4}NIM^{4}_{50}$, **e** $^{2}NIM^{6}_{50}$, **f** $^{4}NIM^{6}_{50}$, **g** $^{6}NIM^{6}_{40}$, **h** $^{2}NIM^{8}_{50}$

the phase distribution became more even and smaller. The PMMA network became more and more finely distributed.

Higher crosslinking of both phases resulted in the development of nanostructured morphology. Figure 3a, b shows the high resolution SEM and TEM (b) images of the nanostructured IPNs with finely dispersed PMMA spherical domains having size in the range of 80 nm. The presence of these smaller domains was due to the direct effect of crosslinking of both phases. Here, the PMMA phase was so compactly arranged with the absence of large domains when compared to the IPNs shown in Fig. 1c–d. Nanometre-sized morphology of the IPNs was a direct result of crosslinking, which can suppress the coarsening process during polymerization and phase separation. In all cases, the formation of a nanometre-sized morphology was accompanied by an enhanced interphase mixing. This particular level of crosslinking was found to produce a finer structure/morphology with some greater regularity (2% in PI and 4% in PMMA).

From the position of the first-order scattering maxima, it is possible to determine the PMMA inter-domain distance for the highly crosslinked PI/PMMA IPN. The inter-domain distance (D) is proportional to the Bragg spacing $a = 2\pi/q_{max}$ so that it is inversely proportional to the scattering vector maxima (q_{max}). The relation between D and a is domain structure dependent [20]. Figure 4 shows the SAXS profile of the highly crosslinked IPN. The inter-domain distances for PMMA calculated from the SAXS data was found to be ~77 nm, which supported the SEM observation of domain size less than 100 nm.

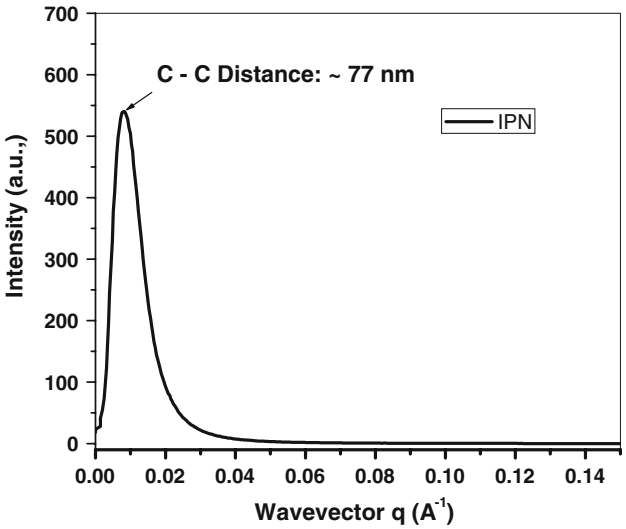

Fig. 4 SAXS profile of PI/PMMA IPN

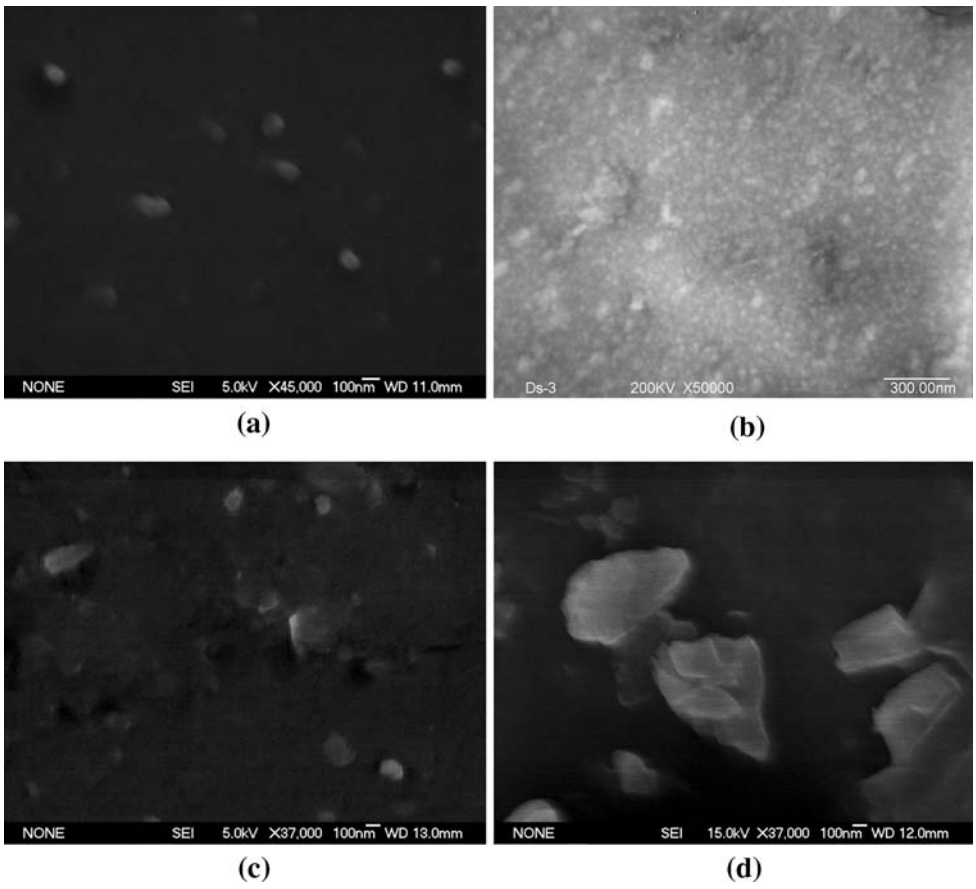

Fig. 3 High-resolution SEM and TEM images of IPNs with nanometre-sized morphology. **a** $^{2}NIM^{4}_{50}$, **b** $^{2}NIM^{4}_{50}$, **c** $^{2}NIM^{6}_{50}$, **d** $^{6}NIM^{6}_{40}$

The cross-linking of the first formed PI network was the main factor contributing to the development of this type of morphology when compared to that of second component. This can be verified by comparing with IPNs in Fig. 1b, c. Here, the PMMA phase was heavily crosslinked (4%) and PI was loosely crosslinked (0.8%). Absence of finer morphology in these IPNs showed the profound influence of the first formed phase and its crosslink density in controlling the morphology of the resulting IPNs. The DMA analysis showed an inward shift in T_g of both phase when the crosslink density of the PI matrix was high and this supported the above fact [19]. The influence of crosslinking in controlling the morphology was found to have a limit. Further crosslinking did not show any considerable effect in the domain dimension of PMMA. This can be seen in Figs. 3c, d and 2e–h. It was also noticed that degree of phase separation increased in full IPN with very high level of crosslinking.

Tensile properties

Tensile properties of the IPN samples are plotted as a function of the overall PMMA content as shown in Figs. 5 and 6. The IPNs showed a gradual change from rubbery to plastic nature with the increase in concentration of PMMA. Tensile strength and modulus were strongly dependent upon the morphology and showed a dramatic change near the 50/50 composition where the system developed a nano-structured morphology. In particular, the tensile strength and modulus showed a lower value in the sea-island region, and a distinct increase when the morphology changed to compact, ordered and smaller PMMA domains having size less than 90 nm and an immediate decrease on the appearance of dual phase morphology. When the PMMA concentration was higher than 30 wt%, tensile strength increased significantly. Elongation at break was found to decrease with the increasing PMMA content due to the low elongation and brittleness of PMMA phase. These results suggest that the nano-structured morphology obtained around 50/50 composition was the key factor that contributed to the mechanical performance of these IPNs. Tensile properties of IPNs are shown in Table 1.

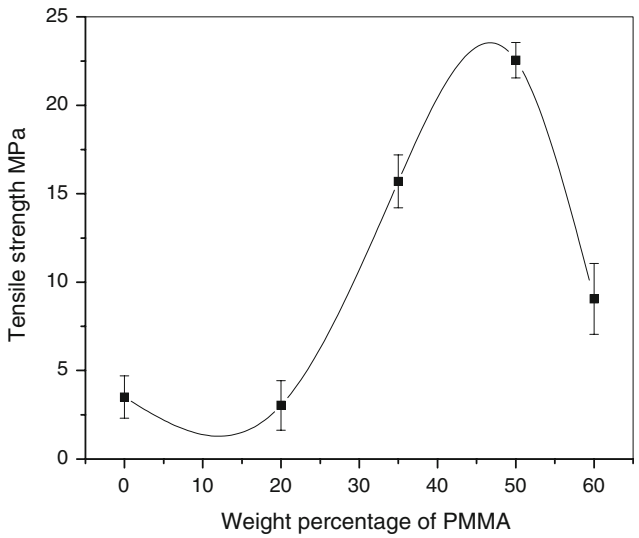

Fig. 5 Effect of wt% of PMMA on tensile strength of full IPNs

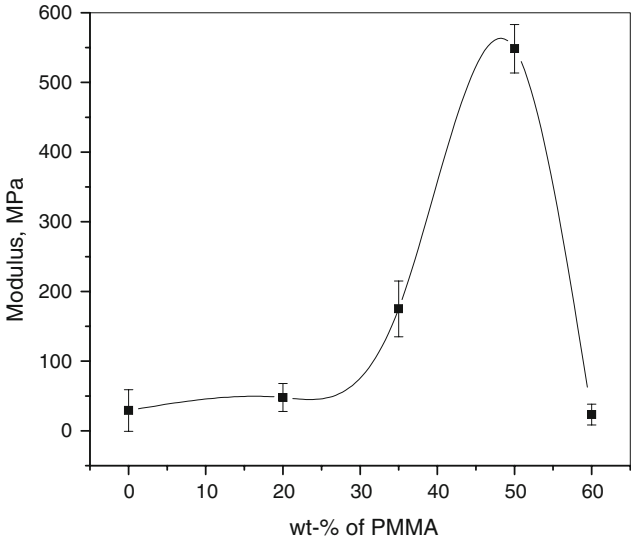

Fig. 6 Effect of wt% of PMMA on modulus of full IPNs

Introduction of crosslinks in PMMA phase was found to improve the mechanical performance of the material. This was due to the higher degree of interpenetration between the PI and PMMA chains during IPN formation. Thus, some degree of enforced miscibility was obtained, which enabled the material to have good mechanical properties. Higher amount of PMMA (more than 55%) was found to reduce the tensile strength.

Effect of crosslink density of PI on the mechanical properties was also studied by preparing IPNs with highly crosslinked PI samples. Tensile strength of these samples is also shown in Table 1. From Fig. 7, it was clear that the crosslink density of PI network had a negative influence on the mechanical properties of these materials. A considerable decrease in tensile strength was observed with the increase in crosslinking degree of the PI phase. However, the effect of crosslink density of PMMA on the mechanical performance of full IPNs was different from that of the PI phase. As shown in Fig. 7, the lower crosslinks in PMMA favours the mechanical properties up to a certain extent, however, higher crosslinking is not desirable. The combination of 2% crosslinker concentration in PI and 4% in PMMA in PI/PMMA IPN led to the development of nano-structured morphology and the said IPN performed better in mechanical measurements.

Table 1 Mechanical properties of full IPNs

Sample	Tensile strength (MPa) (±2)	Elongation at break (%)	Young's modulus (MPa) (±8)	Hardness shore A (±4)
^{2}NR	5.70	804.56	29.09	28
$^{2}NIM^{2}_{20}$	7.84	531.22	83.86	43
$^{2}NIM^{2}_{35}$	19.48	523.72	191.33	55
$^{2}NIM^{2}_{50}$	21.29	403.72	435.39	76
$^{4}NIM^{2}_{20}$	2.07	93.72	191.88	55
$^{4}NIM^{2}_{30}$	3.74	127.89	294.02	59
$^{4}NIM^{2}_{45}$	13.47	239.01	576.77	76
$^{6}NIM^{2}_{25}$	5.58	68.71	4.77	
$^{2}NIM^{4}_{20}$	18.60	561.30	136.09	46
$^{2}NIM^{4}_{35}$	13.96	556.09	230.51	56
$^{2}NIM^{4}_{50}$	21.33	450.39	521.29	77
$^{4}NIM^{4}_{20}$	2.76	105.39	264.74	53
$^{4}NIM^{4}_{35}$	5.39	124.14	430.34	60
$^{4}NIM^{4}_{45}$	11.88	191.84	617.17	76
$^{6}NIM^{4}_{40}$	5.82	89.01	19.09	75
$^{2}NIM^{6}_{50}$	10.08	140.18	802.78	77
$^{4}NIM^{6}_{45}$	12.72	181.51	675.36	81
$^{6}NIM^{6}_{40}$	7.30	70.39	42.2	80
$^{2}NIM^{8}_{50}$	18.45	282.06	592.06	84
$^{0.8}NIM^{4}_{20}$	3.03	607.67	47.82	32
$^{0.8}NIM^{4}_{35}$	15.70	641.22	175.13	55
$^{0.8}NIM^{4}_{50}$	22.55	471.22	548.37	82
$^{0.8}NIM^{4}_{60}$	9.05	90.68	23.40	89

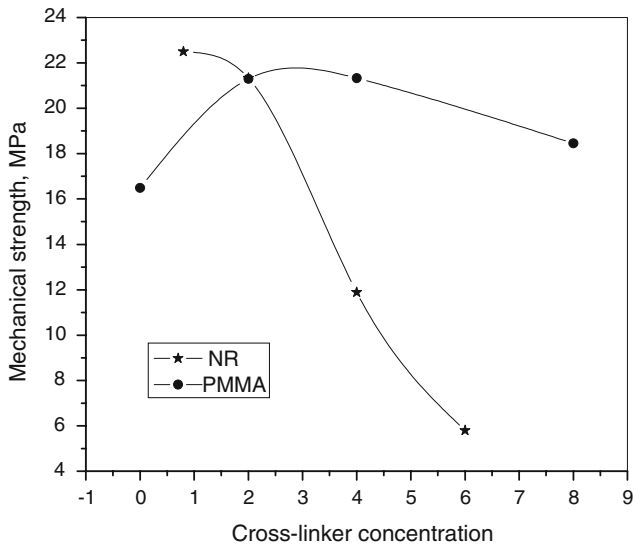

Fig. 7 Effect of crosslink density of PI and PMMA on tensile strength of full IPNs

For a given composition, the elongation at break decreased with the increase of crosslinking in the PI phase. This was due to the reduced chain flexibility of the PI matrix with higher crosslinking. Also crosslinking increased the PMMA entanglement density and interpenetration between the phases. The PMMA network density was found to have only little influence on the elongation at break of full IPNs.

Young's modulus values of full IPNs are also given in Table 1. The Young's modulus of full IPNs was found to increase with the amount of PMMA as shown in Fig. 6. Since modulus is the measure of the stiffness of the material, it was found that the addition of PMMA enhances the stiffness of the material to a large extent. Samples of 50/50 composition showed maximum modulus. Present study also revealed that the Young's modulus increases with the increase in crosslinking of rubber phase. Also crosslink density of the PMMA phase was found to have a pronounced effect in the Young's modulus of full IPNs. The 6% crosslinker concentration in PMMA showed the highest value among the studied samples.

The Shore A hardness values of IPNs are given in Table 1. It was found that shore A hardness increases with the rise in PMMA content.

Theoretical modelling

Various models such as the parallel model, the series model, the Halpin–Tsai equation and the Takayanaki model were made used to study the mechanical behaviour of the IPNs. Kunori and Geil models were used to determine fracture paths (matrix or interface). Figures 8 and 9 show the theoretical and experimental curves of the tensile strength and Young's modulus values, respectively, for the six models. For both tensile strength and modulus, parallel model fits more closely to the experimental values up to 50 wt% of PMMA and then deviates. This may be because both the PI and PMMA phases have a co-continuous morphology above 55 wt% PMMA, rather than having a matrix-dispersed phase morphology. The theoretical curve of Kunori 2 (equation for fracture through matrix) comes closest to the experimental curve compared to the other model. Therefore, it may be concluded that the fracture path is through matrix rather than through the interface. The Kunori 2 values superimpose over parallel model, so lines cannot be distinguished in the figures.

Fractography

Fractography gives information about the mechanism of failure. It is a fact that it is difficult to obtain the exact morphology of the fracture surface at the time of rupture, as there is a large deformation of polymers at the time of failure. There are generally five modes of failure in macromolecular materials:

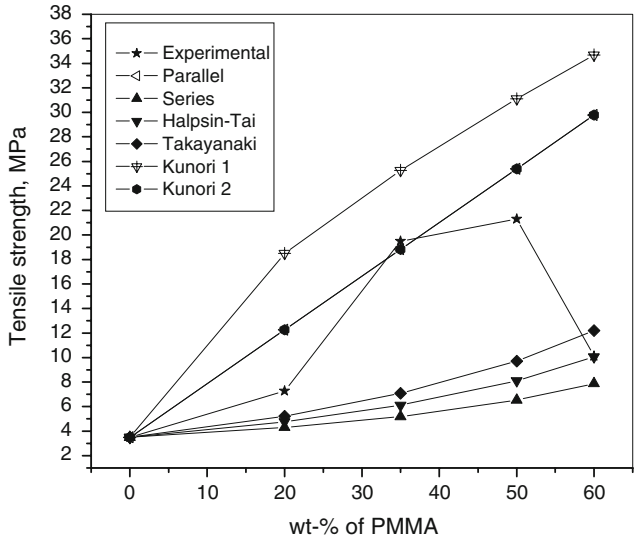

Fig. 8 Model fitting—tensile strength

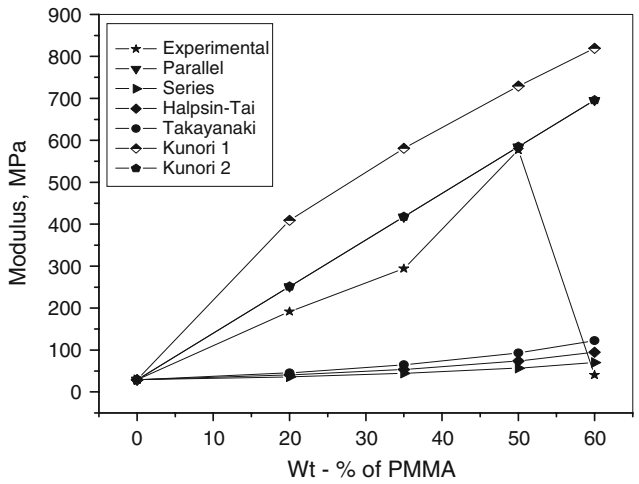

Fig. 9 Model fitting—Young's modulus

i. Brittle failure where a crack is formed and propagated quickly with virtually no plastic deformation prior to failure.
ii. Ductile failure where plastic deformation and voids are produced in the material. The voids join together and failure occurs.
iii. In failure accompanied with crazing, the voids produced are initiated from micro irregularities. The voids are produced because of the movement of the surrounding molecular chains and grows with orientation. The craze gradually changes into a crack and failure occurs.
iv. In boundary failure, failure occurs preferentially at the weakly bonded parts in polymer sample.
v. Fatigue failures are due to the repeated application of stress, which is relatively small compared to tensile strength of the material. The cracks produced due to repeated application of the stress join gradually with the principal crack and failure occurs.

The mode of failure can be studied in detail from the close observation of the fracture surfaces. The strength and properties of the samples can be explained based on failure mode and nature of the fracture surface.

In Fig. 10 samples a and b, the presence of central stress path and layer formation, characteristic of ductile failure was observed. These samples have a more continuous natural rubber matrix and PMMA phase is largely dispersed in rubber matrix. The fracture has occurred due to the breaking of molecular chain after a large amount of elastic deformation. Fibril formation during fracture is generally considered as the evidence of ductile failure with high extent of plastic deformation. Samples a and b did not have fibrils on fracture surface but have peaks, ridges and voids indicating ductile failure with low deformation. In sample c, ribbon like orientation bands, which appear as whitening phenomenon, are observed in the direction of stress. The ribbon like crazes is produced from voids. Sample c has 60% PMMA in it, and a simple brittle failure is observed. The absence of fibrils on the fracture surfaces indicates brittle fracture without any deformation. Therefore, it can be seen that as the amount of PMMA increases the fracture mode changes from ductile to brittle one.

Gas permeability of IPNs

Gas transport properties of IPNs were carried out on membranes of IPNs with oxygen as penetrant gas molecule. We analysed full IPNs with different compositions and crosslink densities for each phases. Values are shown in Table 2. The results showed that transport phenomenon strongly depended upon the crosslink density of PI matrix, composition and morphology obtained during IPN synthesis. It was found that as the concentration of PMMA increases, considerable reduction in permeation is observed for full IPNs. As the crosslink density increases in full IPNs, the material became far less permeable. The results showed that IPN formation was an effective technique that could reduce the permeation of gas molecules through crosslinked polyisoprene matrix. A three- to four-fold decrease in gas transport is observed in the case of full IPNs. Higher crosslink density creates difficult paths for gas molecules and thus reduces permeability. $^{2}NIM^{4}_{50}$ and $^{4}NIM^{4}_{50}$ IPNs are least permeable among the studied specimens. SEM images showed a nanostructured morphology for these IPNs. Nano domains in these IPNs along with highly cross-linked PI matrix resulted in a three to four-fold decrease in transport of oxygen.

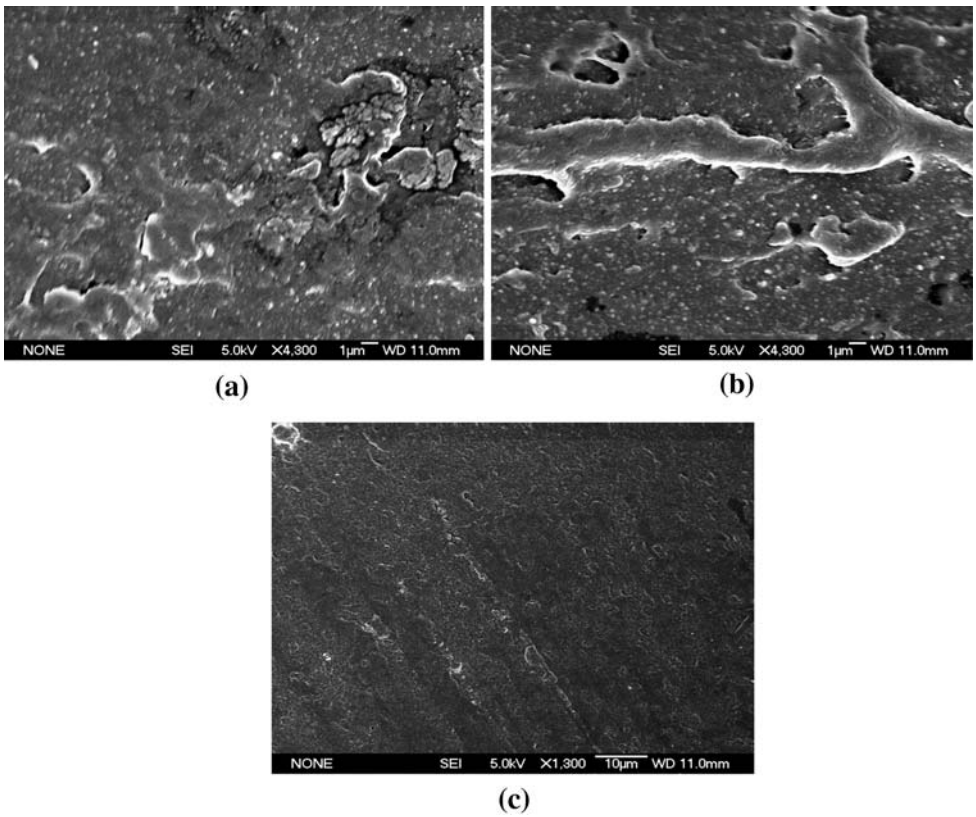

Fig. 10 SEM images of fractured surfaces of IPN samples. **a** $^{0.8}NIM^{4}_{35}$, **b** $^{0.8}NIM^{4}_{50}$, **c** $^{0.8}NIM^{4}_{60}$

Table 2 Gas permeability of IPNs

Samples	Permeation values ($mL/m^2 \times day$)
$^{0.8}NR$	1639.09
$^{2}NIM^{2}_{25}$	949.76
$^{2}NIM^{2}_{50}$	778.64
$^{2}NIM^{4}_{50}$	541.17
$^{4}NIM^{4}_{50}$	461.72
$^{0.8}NIM^{4}_{35}$	1011.01
$^{0.8}NIM^{4}_{50}$	827.43
$^{0.8}NIM^{4}_{60}$	749.87

Thermal stability

Figure 11 shows the TGA curves of pure PI and full IPNs with different composition and crosslink density. It was observed that the presence of crosslinked PMMA in full IPNs has no noticeable effect in the thermal stability of the material. All the IPNs maintain the same thermal behaviour of PI matrix when compared to pure polyisoprene. The highly crosslinked IPNs also showed comparable thermal stability with respect to pure PI.

DSC analysis

DSC curves in Fig. 12 shows two T_gs for all IPNs, a characteristic of phase separated multicomponent polymer systems. The higher T_g corresponding to PMMA was slightly broadened. This broadening was an indication of the presence of a fluctuation in the local glass transition temperature. The presence of highly mobile rubber chains close to rigid PMMA chains induces some flexibility and as a result the PMMA domains highly mixed with rubber chains reach glass transition before those located far from PI chains. This results in the broadening of glass transition.

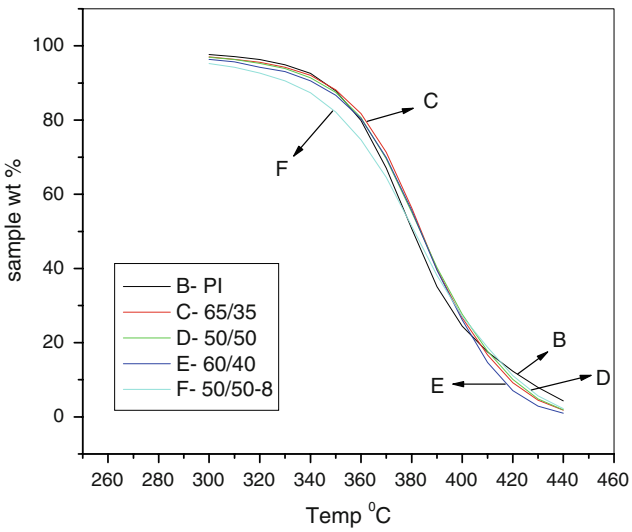

Fig. 11 TGA curves of IPNs

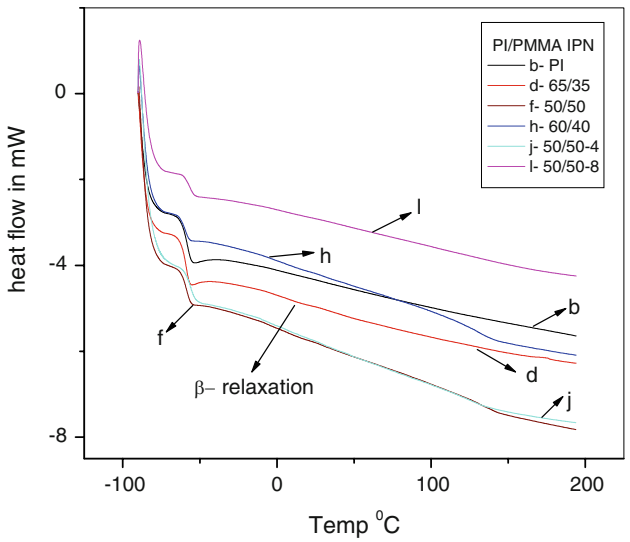

Fig. 12 DSC traces of IPN samples, j and l are samples with different PMMA crosslink density

Beta-relaxation of PMMA can also be seen in the DSC trace of 65/35 sample. At 40/60 PI/PMMA sample, PMMA becomes the major phase and this resulted in a larger transition (PMMA region) as seen in the case of this sample. Higher crosslinking will lead to the spreading of relaxation and this is why no transition is seen in the high temperature region for highly crosslinked PMMA IPN (8%). Nanometre-sized morphology obtained in full IPNs also contributed to the broadening of higher T_g.

Conclusion

Investigations on PI/PMMA full IPNs using SEM, TEM, SAXS, mechanical measurements, TGA, DSC and gas permeability tester are presented. Role of crosslinker concentration and composition on the morphology, miscibility, mechanical, thermal and gas transport properties were studied. Concentrations of PMMA and crosslink density of the first formed phase were found to have an upper hand in controlling the miscibility and morphology of the resulting IPNs. Lower concentration of PMMA (20 and 35 wt%) showed a very fine structure morphology, an indication of certain degree of phase compatibility. DSC of the above composition (35%) also showed a very broad transition arising from the β and α relaxations of PMMA over a temperature range of more than 100 °C. When the concentration of PMMA is increased, both phases tend to become continuous. When the crosslink density of PI phase was increased, PMMA domain size decreased resulting in the development of a nanometre-sized morphology. Also full IPN showed better phase mixing than semi IPN due to greater interpenetration resulting from the PMMA crosslinking. IPN with 50/50 composition showed maximum mechanical strength. All the IPN showed comparable thermal stability with respect to pure PI. Gas permeability of the IPN decreased with rise in crosslinking and concentration of PMMA. Nanostructured IPN showed least permeability among all the studied sample.

Acknowledgement Authors acknowledge the technical support provided by Prof Thomas Russell, (MRSEC) Polymer Science and Engineering, University of Massachusetts, Amherst, USA during this research work. Sivakumar Nagarajan, S. Suriyakala (both from UMASS, Amherst, USA) and Sintomon (CUSAT) are acknowledged for the technical assistance and scientific discussion during the course of this research work.

References

1. Lipatov SY, Alekseeva TT (2007) Adv Polym Sci 208:1
2. Sperling LH (1981) Interpenetrating polymer networks and related materials. Plenum Press, New York
3. Huelck V, Thomas DA, Sperling LH (1972) Macromolecules 5:340
4. Donatelli AA, Sperling LH, Thomas DA (1975) Macromolecules 9:671
5. Widmaier JM, Sperling LH (1981) Macromolecules 15:625
6. Donatelli AA, Sperling LH, Thomas DA (1977) J Appl Polym Sci 21:1189
7. Yeo JK, Sperling LH, Thomas DA (1982) Polym Eng Sci 22:190
8. Fradkin DG, Foster NJ, Sperling LH, Thomas DA (1996) Polym Eng Sci 26:730
9. Duenas JMM, Escuriola DT, Ferrer GG, Pradas MM, Ribelles JLG, Pissis P, Kyritsis A (2001) Macromolecules 34:5525
10. Sanchez MS, Ferrer GG, Cabanilles CT, Duenas JMM, Pradas MM, Ribelles JLG (2001) Polymer 42:10071
11. Alves NM, Ribelles JLG, Tejedor JAG, Mano JF (2004) Macromolecules 37:3735
12. Mathew AP (2001) PhD thesis, Mahatma Gandhi University
13. John J, Nagarajan S, Suryakala R, Klepac D, Yang W, Valic S, Pius A, Thomas S, J Poly Sci Part B (manuscript submitted)
14. Wang M, Paramoda KP, Goh SH (2004) Chem Mater 16:3452
15. Rohman G, Grande D, Laupretre F, Boilean S, Guerin P (2005) Macromolecules 38:7274
16. Pionteck J, Hu J, Schulze U (2003) J Appl Polym Sci 89:1976
17. Mathew AP, Packirisamy S, Thomas S (2000) J Appl Polym Sci 78:2327
18. Mathew AP, Packirisamy S, Radusch HJ, Thomas S (2001) Eur Polym J 37:1921
19. John J, Klepac D, Didovic M, Sandesh CJ, Liu Y, Raju KVSN, Pius A, Valic S, Thomas S, Polymer (manuscript communicated)
20. Canto LB, Torriani IL, Plivelic TS, Hage E Jr, Pessan LA (2007) Polym Int 56:308